BIBECHANA
Vol. 22, No. 2, August 2025, 159-170

ISSN 2091-0762 (Print), 2382-5340 (Online)
Journal homepage: http://nepjol.info/index.php/BIBECHANA
Publisher:Dept. of Phys., Mahendra Morang A. M. Campus (Tribhuvan University)Biratnagar

Multiscale study of interaction between SARS-CoV-2 protein and human receptor complex

Roshan Sigdel, Jhulan Powrel, Nurapati Pantha*, Narayan Prasad Adhikari

Central Department of Physics, Tribhuvan University, Kathmandu, 44618, Nepal
*Corresponding authors. Email: mrnurapati@gmail.com

Abstract

This study explores the binding mechanism of key binding pockets (S19 Q24 A475 and T500 R357) in the Severe Acute Respiratory Syndrome Coronavirus 2 (SARS-CoV-2) spike protein and the Human Angiotensin-Converting Enzyme 2 (hACE2) receptor complex using molecular dynamics (MD) simulations and first-principles calculations. The binding pockets were extracted from the 6LZG protein-protein complex, and the input systems were prepared using CHARMM-GUI for molecular dynamics, PyMOL for structural modifications, and a quantum input generator for first-principles calculations. MD simulations were conducted to assess the stability of the binding pockets and to analyze key interactions, including hydrogen bonding, electrostatic, and van der Waals interactions. Root mean square deviation (RMSD) calculations indicated fluctuations within the system. First-principles calculations, based on density functional theory (DFT) and hybrid functionals, were used to compute the binding energies of residues within the binding pockets, which were found to be negative, suggesting no significant intra-pocket binding. Electronic property analysis revealed that the behavior of key amino acid residues is largely governed by p-orbitals and atomic chemical structure, with minimal influence from crystal symmetry near the Fermi level. Moreover, ethylation of residues A475 was determined to be ineffective in disrupting the interaction between SARS-CoV-2 and the hACE2 receptor.

Keywords
SARS-CoV-2, protein structure, binding pockets, receptor complex, amino acids

Article information
Manuscript received: February 19, 2025; Accepted: May 22, 2025
DOI https://doi.org/10.3126/bibechana.v22i2.75792

1 Introduction

The severe acute respiratory syndrome-like coronavirus (SARS-CoV-2) epidemic that started the COVID-19 pandemic in Wuhan, China, in December 2019 swiftly expanded into a serious global health and economic problem. The virus quickly spread worldwide in 2020, creating widespread illnesses, posing a severe threat to the worldwide population, and intensifying into a global crisis, according to reports of the first human transmission in December 2019. According to the WHO, this disease has been responsible for more than 630 million recorded cases and 6.5 million fatalities worldwide so far [1, 2]. There are many different strains of the big virus family known as coronaviruses. Most viruses affect cats, camels, chickens, and bats. Coronaviruses are unique in that they can spread from one species to another through

“cross-species transmission" or “spillover" meaning that a virus that initially infects one species might change in a way that makes it possible to infect another species. The COVID-19 pandemic started this way; the virus probably originated in bats before spreading to humans via an intermediary animal host. Direct, indirect, and close contact with sick people can spread coronaviruses to others. The virus-containing saliva and respiratory secretions can be expelled by infected people when they exhale, talk, cough, or sneeze. People can then contract the virus by coming into contact with these infected secretions, either by touching contaminated surfaces and then touching their mouth, nose, or eyes or by being close to an infected person who expels infected droplets [3–5].

The first human coronaviruses were detected in the 1960s in patients' nasal discharge linked to the common cold. Named for their crown-like spikes, these viruses caused global outbreaks in the past. Severe acute respiratory syndrome coronavirus (SARS-CoV) emerged in 2002, while Middle East respiratory syndrome coronavirus (MERS-CoV) surfaced in 2012. In 2019, SARS-CoV-2 was identified in China, causing COVID-19 and sparking a pandemic. These coronaviruses are believed to have evolved from bat origins, with some reports suggesting rodent origins for CoV-OC43 and HKU1. Studies indicate CoV-OC43's transmission to humans around 120 years ago, highlighting their prolonged presence in human populations [6, 7].

Coronaviruses are categorized into four genera based on phylogenetic relationships and genomic structure: Alphacoronavirus, Betacoronavirus, Gammacoronavirus, and Deltacoronavirus. Alphacoronavirus and Betacoronavirus mainly infect mammals, including humans, while Gammacoronavirus and Deltacoronavirus target birds. Human coronaviruses HCoV-229E, HCoV-NL63 (Alphacoronavirus), HCoV-OC43, and HCoV-HKU1 (Betacoronavirus) cause common colds. More severe outbreaks, like SARS-CoV, MERS-CoV, and SARS-CoV-2, stem from Betacoronavirus. While both alpha-CoVs and beta-CoVs lead to mild illnesses, SARS-CoV, MERS-CoV, and SARS-CoV-2 can result in severe, life-threatening diseases [4, 8]. Coronaviruses are composed of positive single-stranded RNA and nucleoprotein (N), encased within a lipid bi-layer containing spike glycoprotein (S), membrane protein (M), envelope glycoprotein (E), and hemagglutinin esterase (HE) [4, 8–10]. The RNA genome's length ranges from 26 to 32 kb. SARS-CoV-2, a beta-CoV, exhibits a spherical structure with crown-like spikes measuring 60-140 nm in diameter and 9-12 nm in spike length. SARS-CoV-2 shares about 80 % nucleotide sequence identity with SARS-CoV [4, 9, 11].

Since the emergence of the COVID-19 pandemic, numerous scientists have devoted their efforts to unravelling the complex mechanisms by which SARS-CoV-2 interacts with the hACE2 receptor. Despite significant progress in vaccine development, many people continue to suffer from the virus, highlighting the need for a deeper understanding of the virus's nature and binding mechanisms. Developing more effective vaccines and drugs remains a significant challenge that requires continued research and innovation. [8, 12]. Here, we perform a multiscale study combining molecular dynamics (MD) simulations and Quantum Espresso (QE) calculations to investigate the binding mechanism between SARS-CoV-2 and hACE2. In MD, we analyze hydrogen bonds, van der Waals (VDW), and electrostatic interactions within two key binding pockets: S19 Q24 A475 and R357 T500, where A475 and T500 are SARS-CoV-2 residues, and the rest belong to hACE2. Following this, we use Quantum Expresso codes to conduct quantum mechanical calculations, focusing on the relaxation of these binding sites, estimating the system's total energy and individual residue contributions, and exploring their electronic properties, such as density of states (DOS) and band structures.

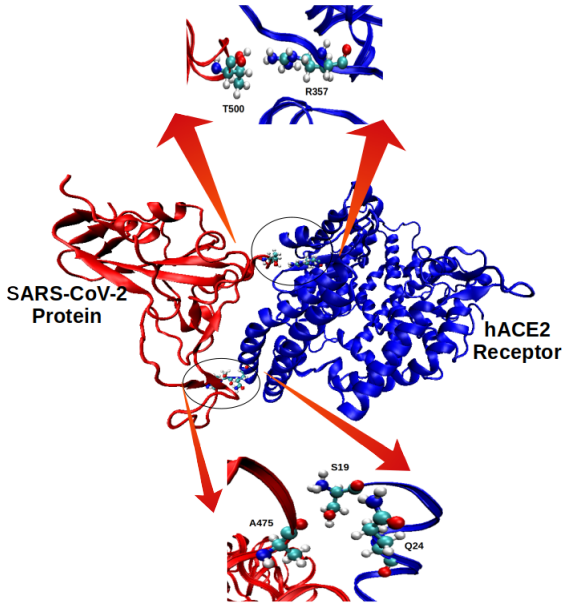

Figure 1: Binding pockets S19 Q24 A475 and R357 T500 in the SARS-CoV-2 protein and hACE2 receptor complex, based on coordinates from the 6LZG.pdb file.

2 Computational Methods

2.1 Molecular Dynamic Simulation

Molecular dynamics (MD) simulations were executed utilizing the NAMD simulation package, employing the 6LZG PDB file from the RCSB Protein Data Bank website, representing the SARS-CoV-2 (Wild type) complex and hACE2 proteins [8, 13]. The simulation system was solvated within a water environment to mimic the cellular milieu, and periodic boundary conditions were imposed to emulate an infinite system. To ensure charge neutrality and maintain the desired pH, a balanced number of positive (Na^+) and negative (Cl^-) ions were introduced. Specifically, for the S19 Q24 A475 binding pocket, 2 Na^+ ions and 2 Cl^- ions were added, and for the R357 T500 binding pocket, 3 Na^+ ions and 4 Cl^- ions were incorporated. The CHARMM36m force field was chosen to describe the interactions in the simulations, providing a comprehensive representation of the system's behaviour. The simulation protocol commenced with energy minimization, spanning 5 ns for each isolated binding pocket and 100 ns for the SARS-CoV-2-hACE2 complex within the NVT ensemble at 310K. Subsequently, a production run of 5ns was carried out for each isolated binding pocket and 100ns for the SARS-CoV-2-hACE2 complex under NPT conditions. The resultant data from the production run underwent Visual Molecular Dynamics (VMD) analysis. Structural stability assessment was performed through root mean square deviation (RMSD) calculations using the Rmsd Trajectory Tool in VMD. The simulation trajectories used VMD analysis tools to identify and analyze bonded and non-bonded interactions.

2.2 First Principles Calculations

An in-depth analysis of the density of states (DOS) and band structures was conducted for two distinct systems. These systems consisted of amino acid residues from hACE-2, SARS-CoV-2, and their constituent amino acids. First-principles calculations were performed using the Quantum ESPRESSO algorithm. The electronic exchange and correlation effects were incorporated into the system through the PBEsol functional developed by John P. Perdew. This hybrid density functional, employed by PBEsol, combines the exchange from a Hartree-Fock calculation with the correlation from a density functional description, which are two distinct types of functionals in density functional theory (DFT) [14].

Andrea Dal Corso's projector augmented wave (PAW) pseudopotential, obtained from the Quantum ESPRESSO website, was used to replace the complex effects of the motion of an atom's core (i.e., non-valence) electrons with an effective potential. This ensured that only the chemically active valence electrons were explicitly considered through-

out the entire calculation [15]. The structure was optimized using the Broyden-Fletcher-Goldfarb-Shanno (BFGS) scheme and was allowed to relax until the total energy change between two successive self-consistent field (SCF) steps was less than 10^{-7} Ry, and each component of the acting force was below 10^{-4} Ry/Bohrs [16].

A degauss value of 0.001 Ry was used, with "occupation" fixed and "smearing" applied in various systems depending on the number of electrons present. The David diagonalization method was employed with the "plain" mixing mode and a mixing value of 0.4 to ensure self-consistency. To prepare for subsequent calculations, the optimal convergence values for the kinetic energy cutoff and k-point sampling were determined. These choices were made to enhance the accuracy of the calculations while minimizing computational expenses. Since the system lacked a crystalline nature, it was necessary to transform it into a crystalline arrangement by encapsulating it within a cell. This adaptation was required to enable the accurate execution of first-principles calculations.

Since the system's crystalline size is not fixed for band calculations, a k-path was generated using the "SeeK-path" tool from Material Cloud [17], following the suggested path Γ–X | Y–Γ–Z | R–Γ–T | U–Γ–V | Γ–X' | Y'–Γ–Z' | R'–Γ–T' | U'–Γ–V', where Γ represents the Brillouin zone center, and other points denote symmetry-related locations within the reciprocal space. The band structure analysis primarily focuses on the R–Γ–T segment, with corresponding k-points.

3 Results and Discussion

3.1 Root-Mean-Square Deviation(RMSD)

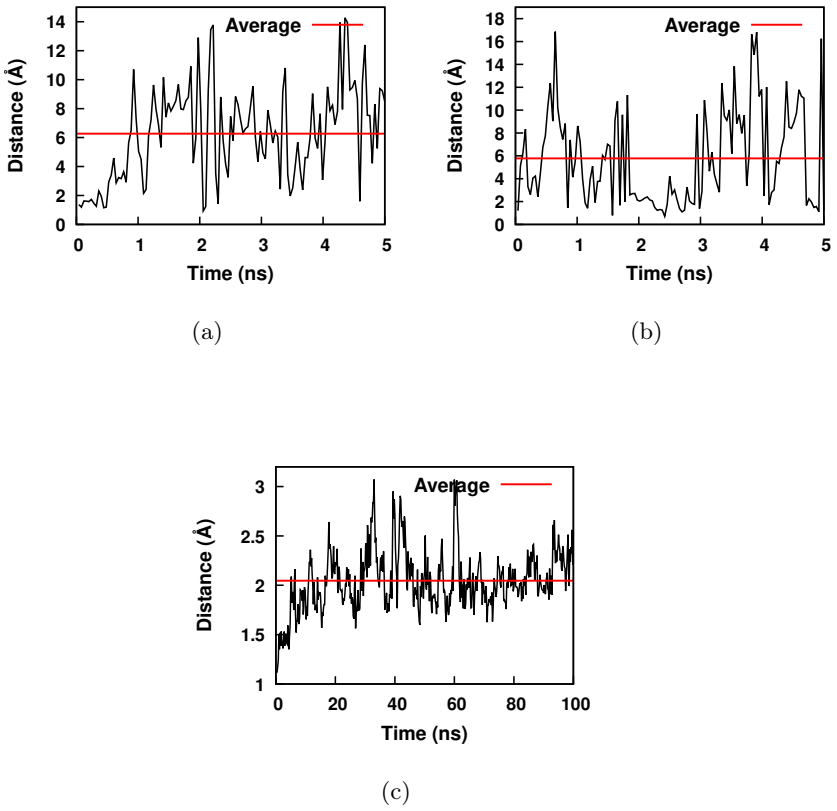

Figure 2: Time evolution of RMSD of the isolated system of S19 Q24 A475 (2a) and T500 R357 (2b) binding pockets of S protein and human ACE2 complex during the 5 ns simulation run, and of the system containing SARS-CoV-2 spike protein and hACE2 receptor complex during the 100 ns simulation run (2c).

The figure in 2 illustrates the RMSD values for a range of systems, including isolated single binding pockets (S19 Q24 A475, and T500 R357) within the S protein and human ACE2 complexes, as well as the complete S protein and human ACE2 complexes. Specifically, the RMSD fluctuations for in-

dividual isolated binding pockets, such as S19 Q24 A475 and T500 R357 within the S protein and human ACE2 complexes, exhibit variations spanning 14.25 Å to 0.91 Å and 16.85 Å to 0.74 Å, respectively. On the other hand, the RMSD fluctuations for the S protein and hACE2 complexes themselves range from 3.78 Å to 1.115 Å. Regarding average RMSD values, the isolated binding pockets (S19 Q24 A475 and T500 R357) and the S protein and hACE2 complexes demonstrate values of 6.27 Å, 5.78 Å, and 2.05 Å, respectively. Further examination of the RMSD values over time reveals that the isolated system containing only binding pockets (S19 Q24 A475 and T500 R357) fluctuations start at 1.35 Å and 1.19 Å, respectively, and fluctuate in between their respective maximum and minimum values. The most pronounced fluctuations occur between 1.9 ns and 2.3 ns, as well as between 3.99 ns and 4.6 ns for S19 Q24 A475, and between 0.36 ns and 0.85 ns, as well as between 3.75 ns and 4 ns for T500 R357. Eventually, the RMSD values stabilize at a relatively constant level. Similarly, the RMSD values for the S protein and hACE2 complexes initially fluctuate, with significant variations between 26.8 ns and 36.8 ns and between 59.6 ns and 62 ns. Ultimately, these values also reach a steady state. The results indicate that both the S protein and hACE2 complexes and the isolated system containing only binding pockets S19 Q24 A475 and T500 R357 maintain relatively consistent RMSD values, suggesting structural stability in the molecular dynamics simulation. The more significant fluctuations observed in the isolated system can be attributed to the absence of interactions with other amino acids in the S protein and hACE2 complexes.

3.2 Hydrogen Bonds

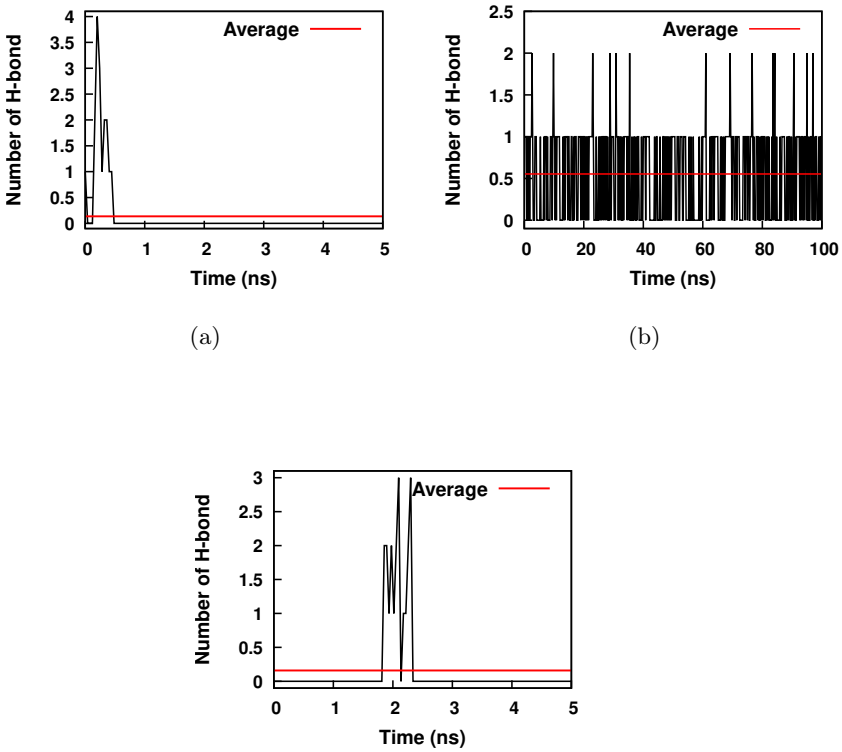

Figure 3: Time evolution of the number of hydrogen bonds (H-bonds) formed between S protein and hACE2 (S19 Q24 A475 and T500 R357) for the isolated system during 5ns simulation runs (3a), and (3c) and the system containing SARS-CoV-2 Spike protein and hACE2 receptor complex for pocket S19 Q24 A475 during 100 ns simulation runs (3b).

To calculate the number of hydrogen bonds between amino acid residues of binding pockets A475 S19 Q24 and T500 R357 of the SARS-CoV-2 S protein and the ACE2 receptor, we utilized the VMD extension Hydrogen Bonds with a 3.5 Å cut-off distance for hydrogen bond formation.

Table 1: Occupancy Percentage of Hydrogen Bonds in the S19 Q24 A475 and T500 R357 Binding Pocket of the S Protein-hACE2 Complex

Hydrogen Bonds	Occupancy %
For S19 Q24 A475 Binding Pocket	
SER19-Side—ALA475-Side	1.60%
ALA475-Main—GLN24-Main	0.80%
ALA475-Main—GLN24-Side	2.40%
SER19-Main—ALA475-Main	4.00%
SER19-Main—ALA475-Side	4.00%
GLN24-Main—ALA475-Side	0.80%
For S19 Q24 A475 Binding Pocket from Total SARS-CoV-2 Spike Protein-hACE2 Complex	
SER19-Side—ALA475-Main	41.12%
SER19-Main—ALA475-Main	7.19%
GLN24-Side—ALA475-Main	6.99%
For T500 R357 Binding Pocket	
ARG357-Main—THR500-Main	3.20%
ARG357-Main—THR500-Side	6.40%
THR500-Side—ARG357-Side	0.80%
ARG357-Side—THR500-Main	2.40%
ARG357-Side—THR500-Side	3.20%

Figure 3 illustrates the dynamic changes in hydrogen bond counts for various binding pockets within the S protein and human ACE2 complex. The isolated systems of S19 Q24 A475 and T500 R357 exhibit fluctuating hydrogen bond counts ranging from 0 to 4 and 0 to 3, respectively. Similarly, the binding pocket within the SARS-CoV-2 spike protein and hACE2 receptor complex, namely S19 Q24 A475, experiences hydrogen bond fluctuations from 0 to 2. Notably, no hydrogen bonds were observed between amino acid residues T500 and R357 in the T500 R357 binding pocket of the SARS-CoV-2 spike protein and hACE2 receptor complex. The total number of hydrogen bonds between the hACE2 receptor and S protein amino acid residues for the isolated systems of S19 Q24 A475 and T500 R357 binding pockets are 6 and 5, respectively. The corresponding binding pockets within the SARS-CoV-2 spike protein and hACE2 receptor complex are 3 and 0, respectively. Detailed hydrogen bond occupancy percentages are summarized in Table 1.

From Table 1, the isolated binding pockets exhibit minimal hydrogen bonding with very low occupancy percentages. This indicates that the hydrogen bonds involving amino acids S19, Q24, and A475 are insignificant enough to confirm stable binding. However, the same binding pocket comprising S19, Q24, and A475 in the complete complex shows a significant hydrogen bond contribution, particularly between SER19 (side chain) and ALA475 (main chain). This discrepancy arises because isolating a specific binding pocket by removing all other binding pockets alters the system's environment, demonstrating that amino acids from other binding pockets also influence the hydrogen bonding within a given binding pocket.

Similarly, the binding site involving T500 and R357 in the complete complex does not exhibit any hydrogen bonding. However, small hydrogen bonds are observed in the system containing only the T500–R357 binding pocket, isolated from all other binding sites. This behaviour reinforces that interactions between binding pockets are critical in modulating hydrogen bonding within individual pockets.

3.3 VDW or Electrostatic Interactions

Electrostatic and van der Waals interactions are critical non-covalent interactions prevalent in biological systems. These interactions are crucial in both intermolecular and intramolecular binding between biomolecules. In proteins, charged amino acids attract or repel each other due to electrostatic interactions. Meanwhile, van der Waals interactions occur due to the temporary asymmetry of electron density around an atom, which creates a dipole moment. This dipole moment is responsible for the attractive force at longer distances and the repulsive force at shorter distances.

Our study analyzed VDW, or electrostatic interactions between amino acid residues within two binding pockets (S19 Q24 A475 and T500 R357) found in the spike protein and hACE2 receptor complex. We examined the electrostatic and van der Waals forces between these residues using an isolated system approach. We compared the results of our analysis with those obtained from systems containing

the S19 Q24 A475 and T500 R357 binding pockets of the SARS-CoV-2 spike protein and hACE2 receptor complex, respectively. In both the isolated system and the system containing the SARS-CoV-2 spike protein and hACE2 receptor complex, the interactions among amino acid residues within the S19 Q24 A475 and T500 R357 binding pockets are characterized by significant non-bonded interaction energies, which are primarily composed of van der Waals and electrostatic contributions. For the system involving the SARS-CoV-2 spike protein and hACE2 receptor complex, the average electrostatic contribution, van der Waals interaction, and non-bonded interaction energies are (-12.64 ± 0.19) kcal/mol, (-0.9996 ± 0.043) kcal/mol, and (-13.64 ± 0.18) kcal/mol, respectively, for the S19 Q24 A475 binding pocket; and (1.61 ± 0.13) kcal/mol, (-0.93 ± 0.02) kcal/mol, and (0.675 ± 0.124) kcal/mol, respectively, for the T500 R357 binding pocket. On the other hand, the isolated system of the S19 Q24 A475 and T500 R357 binding pockets shows negligible electrostatic contribution, van der Waals interaction, and non-bonded interaction energies. The average values for these interactions are (-5.46 ± 1.92) kcal/mol, (-0.022 ± 0.042) kcal/mol, and (-5.48 ± 1.91) kcal/mol, respectively, for the S19 Q24 A475 binding pocket; and (-8.104 ± 1.797) kcal/mol, (0.017 ± 0.0788) kcal/mol, and (-8.09 ± 1.76) kcal/mol, respectively, for the T500 R357 binding pocket.

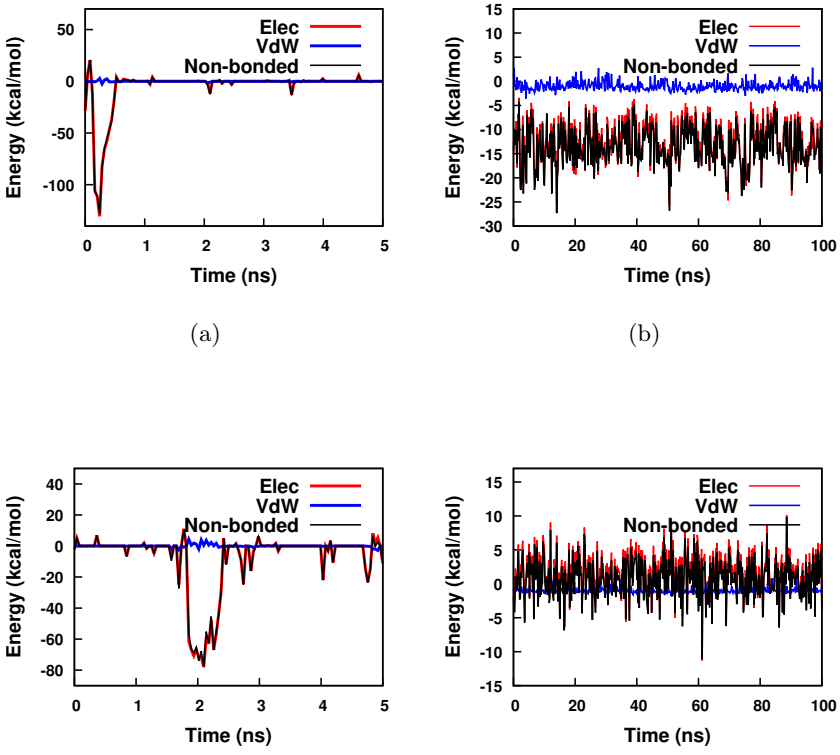

Figure 4: Variation of electrostatic (Elec) and van der Waals (vdW) interaction energies between the amino acid residue of S protein and amino acid residue of hACE2 for the isolated system of S19 Q24 A475 and T500 R357 binding pocket, (4a) and (4c), and for the system containing SARS-CoV-2 Spike protein and hACE2 receptor complex for S19 Q24 A475 and T500 R357 binding pocket, (4b) and (4d).

The nonbonded interaction in both the isolated systems and the system containing the SARS-CoV-2 spike protein and hACE2 receptor complex are primarily driven by van der Waals and electrostatic interactions. However, the magnitudes of nonbonded interaction energies are higher in the latter case. The van der Waals interaction remains relatively stable by examining the electrostatic, van der Waals, and total nonbonded interaction plot in Figure 4. At the same time, fluctuations are more pronounced in the electrostatic interaction. Consequently, these fluctuations lead to considerable variations in the overall nonbonded interaction energy, the sum of van der Waals and electrostatic interactions. Notably, these fluctuations are less intense in the isolated systems of binding pockets within the S protein and human ACE2 complex compared to the system containing the SARS-CoV-2 spike pro-

tein and hACE2 receptor complex.

3.4 Energy Calculations

We employed an SCF input file for a comprehensive quantum mechanical analysis, calculating the total energy alongside Fermi energy, Kohn-Sham states, and energy eigenvalues. Our objective was to uncover the binding energy within two specific binding pockets of the SARS-CoV-2 spike protein and hACE2 receptor complex. This was achieved through a range of first-principles calculation setups utilizing Quantum ESPRESSO, adjusting lattice parameters (a, b, and c) based on system size (Table 2).

Table 2: Lattice parameters, crystal structures, and total energies of various systems for two binding pockets.

System	Lattice Parameters (a=b=c) in Å	Crystal Structure	Total Energy of Systems of binding pockets (Ry)
Ethane	-	-	-42.8747
For S19 Q24 A475 Binding Pocket			
S19 Q24 A475	11.9112	Cubic	-544.2074
S19 Q24	11.9112	Cubic	-412.7575
S19	5.07	Cubic	-172.6133
Q24	8.1787	Cubic	-240.1767
A475	4.9275	Cubic	-131.4759
Ethylated A475	6.4988	Cubic	-172.4018
Ethane	5.5738	Cubic	-42.8747
For T500 R357 Binding Pocket			
T500 R357	15.9037	Cubic	-471.5230
R357	11.790	Cubic	-278.4724
T500	5.5738	Cubic	-193.1114
Ethane	5.5738	Cubic	-42.8747

The binding energy of each binding pocket can be determined by utilizing the ground state energy values of the individual amino acid residues of the SARS-CoV-2 spike protein and the hACE2 receptor. The binding energy for the systems is calculated using the following equation:

- Binding energy for S19 Q24 A475 binding pocket

$$E_{binding} = E_{S19}+E_{Q24}+E_{A475}-E_{S19-Q24-A475} \quad (1)$$

$$E_{binding} = -0.0584Ry$$

- Binding energy for T500 R357 binding pocket

$$E_{binding} = E_{T500} + E_{R357} - E_{T500-R357} \quad (2)$$

$$E_{binding} = -0.0607Ry$$

- Binding energy for Ethylated A475

$$E_{binding} = E_{A475} + E_{C_2H_6} - E_{EthylatedA475} \quad (3)$$

$$E_{binding} = -1.9488Ry$$

Where, E_{S19}, E_{Q24}, and E_{R357} represent the energies of the amino acid residues of the hACE2 receptor, E_{A475} and E_{T500} represent the energies of the amino acid residues of the SARS-CoV-2 spike protein, and ethylated energy of E_{A475} is $E_{EthylatedA475}$. Additionally, $E_{S19-Q24-A475}$ and $E_{T500-R357}$ represent the total system energies of each binding pockets.

Understanding the interaction between the SARS-CoV-2 spike protein and the hACE2 receptor complex is vital for understanding viral infection mechanisms, but predicting amino acid binding accurately was challenging due to the absence of a fixed geometry. Analysis of the S19 Q24 A45 pocket revealed that the calculated binding energy of -0.0584 Ry is negative, suggesting no binding, which contradicts the actual situation within the pocket. In reality, the amino acid residues are bound through hydrogen bonds, Van der Waals forces, and electrostatic interactions [8]. Similar inconsistencies are seen in pockets T500 R357 (with binding energy -0.0607 Ry), which bind via Van der Waals or electrostatic interactions. Factors like body fluids, temperature, and bulk protein interactions that are unaccounted for in our system can influence binding. Our isolated site approach might lead to negative binding energies, indicating unbinding. The effect of ethylation was investigated on residue A475. The A475 ethylated complex was -1.9488 Ry in binding energy, indicating a state of instability. The ethylation modification did not succeed in enhancing the stabilization of the hACE2-SARS-CoV-2 binding complex, suggesting that the strategy is ineffective in destabilizing the binding interface between the amino acid residues of the SARS-CoV-2 protein and the hACE2 receptor complex.

3.5 Density of States (DOS) And Bands

The band structure of solids, stemming from quantum forces on isolated atoms, governs their electronic and optical traits, pivotal in materials science. Electrons adhere to Pauli exclusion, occupying valence bands while leaving the conduction band accessible. The band gap, devoid of orbitals, separates them and emerges from electron-ion interactions. Materials are classified based on the band gap: conductors (small/zero gap), semiconductors (0.1-4 eV), and insulators (>4 eV). Conductors allow easy electron flow, semiconductors suit electronics, and insulators hinder electricity [18]. The density of States (DOS) characterizes available quantum states in a solid's energy range, impacting electronic, transport, and magnetic traits. Calculating DOS reveals energy band distribution, shedding light on electron behaviour.

3.5.1 For S19 Q24 A475 Binding Pocket

The figures (5a and 5b), (5c and 5d), (5e and 5f), (5g and 5h), (5i and 5j), and (5k and 5l) depict the band and DOS structures, along with PDOS highlighting orbital and atomic contributions, for the hACE2 receptor's amino acid residue (S19 and Q24), SARS-CoV-2's amino acid residue (A475), S19 Q24, S19 Q24 A45, and ethylated A475 respectively. Starting with S19, it exhibits n-type semiconductor behaviour with a band gap of 2.52 eV. The presence of conduction bands close to the Fermi surface suggests it can act as an electron donor. The band contributions in the conduction and valence bands, as seen in Figures 5a and 5b, are primarily attributed to the p-orbital of carbon and nitrogen atoms, respectively. The band structures near the Fermi level do not significantly vary with high symmetric points, indicating that crystal symmetry does not significantly affect electronic states. Moving on to the Q24 system, it falls within the wide energy gap semiconductor category with a band gap of 3.3798 eV. Like S19, the p-orbital of carbon and oxygen atoms predominantly contributes to the conduction band, while the p-orbital of oxygen mainly influences the valence band. Like before, the band structures around the Fermi level remain relatively unchanged across high symmetric points. A475, on the other hand, exhibits n-type semiconductor behaviour with a band gap of 2.4808 eV. Its conduction bands' proximity to the Fermi level facilitates electron movement, making it an effective electron donor. The p-orbitals of carbon and nitrogen atoms play a significant role in the conduction and valence bands, similar to S19 and Q24. Again, the band structures near the Fermi level show minimal variation with high symmetric points. In the S19 Q24 system, the interaction between S19 and Q24 results in a system with a band gap of 3.0851 eV. This places it in the wide energy gap semiconductor regime. The p-orbital of carbon atoms and some contribution from oxygen are notable in the conduction band, while the valence band's behaviour is akin to that of S19 and Q24. Despite the binding, the electronic properties align more with Q24, and the band structures near the Fermi level remain largely consistent. The S19 Q24 A475 system also demonstrates semiconductor characteristics with a band gap of 2.2652 eV. The band contributions in the conduction and valence bands resemble those of the individual amino acids. Importantly, after the interaction, the system's semiconductor nature still aligns with that of the hACE2 receptor, indicating a shift in properties towards hACE2 characteristics. The band structures around the Fermi level exhibit no significant changes due to the interaction. Finally, ethylated A475 exhibits p-type semiconductor behaviour with a band gap of 3.4036 eV. The valence band's proximity to the Fermi level indicates electron acceptance characteristics. Interestingly, the ethylation of A475 transforms its properties from n-type to wide energy gap p-type semiconductors. Despite this shift, the band contributions from the p-orbitals of carbon and oxygen atoms persist, and the band structures near the Fermi level display slight variations across high symmetric points. This suggests that ethylation does not dramatically impact the electronic structure at these energy levels.

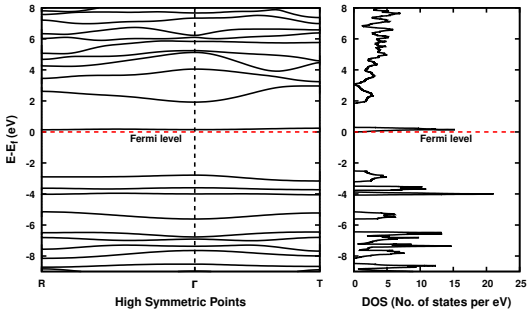
E-E$_f$ (eV)
Fermi level
R
Γ
T
High Symmetric Points
DOS (No. of states per eV)

(a)

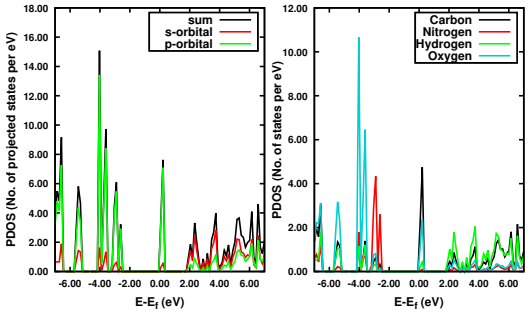
PDOS (No. of projected states per eV)
sum
s-orbital
p-orbital
E-E$_f$ (eV)
PDOS (No. of states per eV)
Carbon
Nitrogen
Hydrogen
Oxygen

(b)

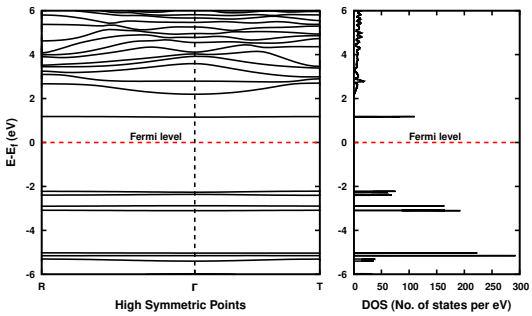
E-E$_f$ (eV)
Fermi level
R
Γ
T
High Symmetric Points
DOS (No. of states per eV)

(c)

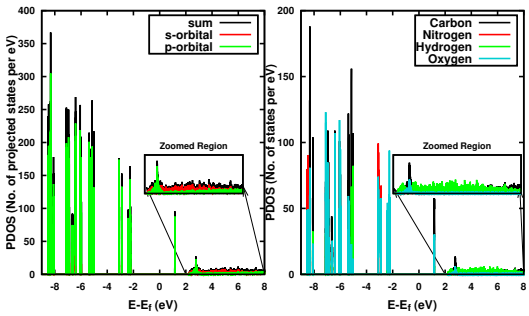
PDOS (No. of projected states per eV)
sum
s-orbital
p-orbital
Zoomed Region
E-E$_f$ (eV)
PDOS (No. of states per eV)
Carbon
Nitrogen
Hydrogen
Oxygen

(d)

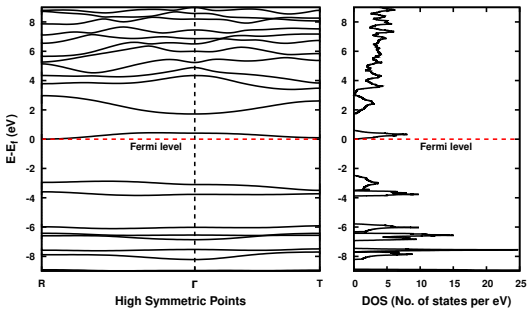
E-E$_f$ (eV)
Fermi level
R
Γ
T
High Symmetric Points
DOS (No. of states per eV)

(e)

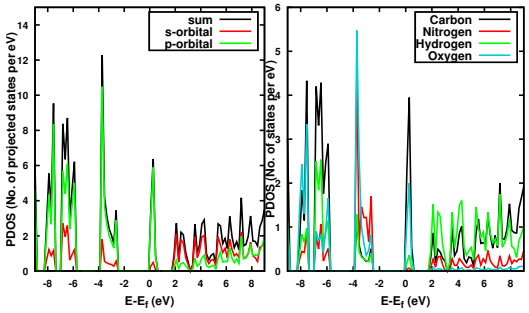
PDOS (No. of projected states per eV)
sum
s-orbital
p-orbital
E-E$_f$ (eV)
PDOS (No. of states per eV)
Carbon
Nitrogen
Hydrogen
Oxygen

(f)

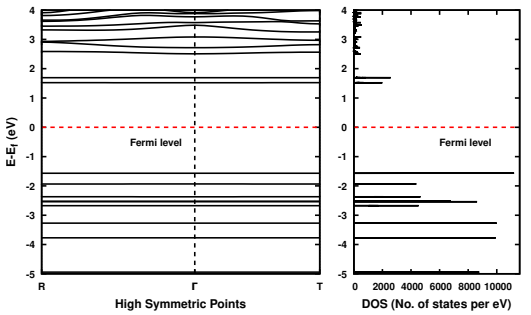
E-E$_f$ (eV)
Fermi level
R
Γ
T
High Symmetric Points
DOS (No. of states per eV)

(g)

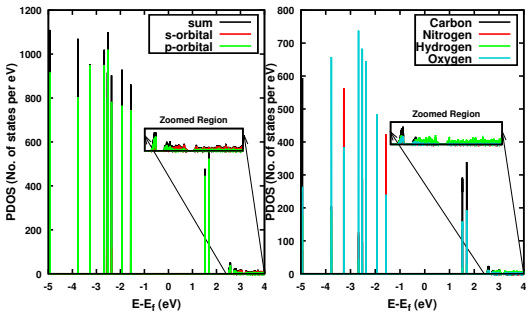
PDOS (No. of states per eV)
sum
s-orbital
p-orbital
Zoomed Region
E-E$_f$ (eV)
PDOS (No. of states per eV)
Carbon
Nitrogen
Hydrogen
Oxygen

(h)

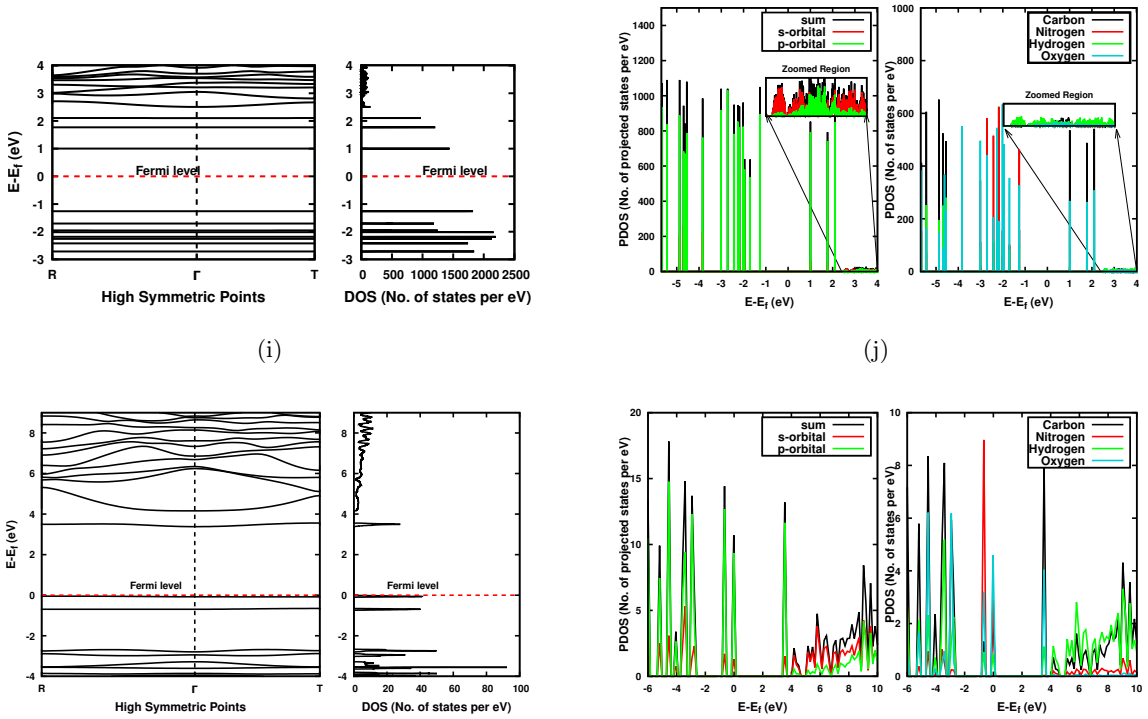

Figure 5: Figures (5a), (5c), (5e), (5g), (5i), and (5k) illustrate the Band and DOS structures for the S19, Q24, A475, S19 Q24, S19 Q24 A475, and Ethylated A475 systems, respectively. Figures (5b), (5d), (5f), (5h), (5j), and (5l) display the Orbital-projected density of states and Atom-projected density of states for the S19, Q24, A475, S19 Q24, S19 Q24 A475, and Ethylated A475 systems.

3.5.2 For T500 R357 Binding Pocket

R357 has a wide energy gap n-type semiconductor nature with a 3.3505 eV band gap, featuring bands at the Fermi level. Band contributions near the Fermi level stem mainly from p-orbitals, Oxygen, and Nitrogen atoms. The preserved band structure symmetry suggests a critical role in the SARS-CoV-2 binding mechanism. The semi-metallic nature and Fermi-level states suggest potential interactions with other molecules. T500, a p-type semiconductor, possesses a 2.881 eV band gap with Carbon and Nitrogen-driven conduction and valence bands near the Fermi level. Symmetry analysis reveals minimal changes near the Fermi level, implying consistent electronic properties. T500 R357 exhibits a 3.4137 eV band gap with n-type semiconductor behaviour, mirroring hACE2's properties post-interaction. Band contributions involve p-orbitals, Carbon, Nitrogen, and Oxygen atoms. The consistent band structure near the Fermi level hints at the modification after binding, indicating potential for drug design.

4 Conclusions

Our study involved three molecular dynamics simulations: two on isolated binding pockets (S19 Q24 A475 and T500 R357) and one on the full SARS-CoV-2 spike protein-hACE2 receptor complex. These simulations (5ns, 5ns, and 100ns) aimed to reveal binding mechanisms by assessing stability and amino acid interactions, including hydrogen bonds, electrostatic, and van der Waals forces. RMSD values confirmed stability, with the isolated S19 Q24 A475 system averaging 6.27 Å, 5.78 Å for T500 R357 system, and the full complex averaging 2.05 Å. Non-bonded interactions, particularly van der Waals and electrostatic forces were stronger in the full complex than in isolated pockets, with significant electrostatic fluctuations.

First-principles calculations revealed negative binding energies for specific amino acid interactions, though real-world conditions could alter these results. Ethylation of A475 was found to have minimal impact on binding. Density functional theory analyses highlighted the electronic properties of key amino acids, showing strong p-orbital contributions with limited crystal symmetry effects near the Fermi level. These findings deepen our understanding of the binding mechanisms between SARS-CoV-2 and hACE2, offering valuable insights for developing therapeutics aimed at disrupting viral interactions.

Acknowledgements

R. Sigdel sincerely expresses his gratitude to the University Grants Commission (UGC) for its financial support. The authors acknowledge the computing facilities provided by the Tribhuvan University Research Coordination and Development Council (RCDC) through the National Priority Grants TU-NPAR-077/78-ERG-14.

References

[1] Ben Hu, Hua Guo, Peng Zhou, and Zheng-Li Shi. Characteristics of sars-cov-2 and covid-19. *Nature Reviews Microbiology*, 19(3):141–154, 2021.

[2] World Health Organization. Who coronavirus (covid-19) dashboard. URL https://covid19.who.int/, 2022. [Online: accessed 13-November-2022].

[3] Matteo Di Nardo, Grace van Leeuwen, Alessandra Loreti, Maria Antonietta Barbieri, Yit Guner, Franco Locatelli, and Vito Marco Ranieri. A literature review of 2019 novel coronavirus (sars-cov-2) infection in neonates and children. *Pediatric Research*, 89(5):1101–1108, 2021.

[4] Anshumali Mittal, Kavyashree Manjunath, Rajesh Kumar Ranjan, Sandeep Kaushik, Sujeet Kumar, and Vikash Verma. Covid-19 pandemic: Insights into structure, function, and hace2 receptor recognition by sars-cov-2. *PLoS Pathogens*, 16(8):e1008762, 2020.

[5] Koichi Yuki, Miho Fujiogi, and Sophia Koutsogiannaki. Covid-19 pathophysiology: A review. *Clinical Immunology*, 215:108427, 2020.

[6] Ding X Liu, Jia Q Liang, and To S Fung. Human coronavirus-229e, -oc43, -nl63, and -hku1 (coronaviridae). In *Encyclopedia of Virology*, pages 428–440. Elsevier, 2021.

[7] Zi-Wei Ye, Shuofeng Yuan, Kit-San Yuen, Sin-Yee Fung, Chi-Ping Chan, and Dong-Yan Jin. Zoonotic origins of human coronaviruses. *International Journal of Biological Sciences*, 16(10):1686, 2020.

[8] Qihui Wang, Yanfang Zhang, Lili Wu, Sheng Niu, Chunli Song, Zengyuan Zhang, Guangwen Lu, Chengpeng Qiao, Yu Hu, Kwok-Yung Yuen, et al. Structural and functional basis of sars-cov-2 entry by using human ace2. *Cell*, 181(4), 2020.

[9] Fang Li. Structure, function, and evolution of coronavirus spike proteins. *Annual Review of Virology*, 3:237–261, 2016.

[10] W Joost Wiersinga, Andrew Rhodes, Allen C Cheng, Sharon J Peacock, and Hallie C Prescott. Pathophysiology, transmission, diagnosis, and treatment of coronavirus disease 2019 (covid-19): A review. *JAMA*, 324(8):782–793, 2020.

[11] Melissa R Gitman, Maryia V Shaban, Alberto E Paniz-Mondolfi, and Emilia M Sordillo. Laboratory diagnosis of sars-cov-2 pneumonia. *Diagnostics*, 11(7):1270, 2021.

[12] Rajendra P Koirala, Bidhya Thapa, Shyam P Khanal, Jhulan Powrel, Rajendra P Adhikari, and Narayan P Adhikari. Binding of sars-cov-2/sars-cov spike protein with human ace2 receptor. *Journal of Physics Communications*, 5(3):035010, 2021.

[13] Rcsb pdb, protein data bank. URL https://www.rcsb.org/structure/6LZG, 2023. [Online: accessed 02-February-2023].

[14] John P Perdew, Adrienn Ruzsinszky, Gábor I Csonka, Oleg A Vydrov, Gustavo E Scuseria, Lucian A Constantin, Xiaolan Zhou, and Kieron Burke. Restoring the density-gradient expansion for exchange in solids and surfaces. *Physical Review Letters*, 100(13):136406, 2008.

[15] Andrea Dal Corso. Pseudopotentials periodic table: From h to pu. *Computational Materials Science*, 95:337–350, 2014.

[16] Bernd G Pfrommer, Michel Côté, Steven G Louie, and Marvin L Cohen. Relaxation of crystals with the quasi-newton method. *Journal of Computational Physics*, 131(1):233–240, 1997.

[17] Material cloud tools: Seekpath, input generator, and structure visualizer. URL https://www.materialscloud.org/work/tools, 2023. [Online: accessed 02-February-2023].

[18] John Singleton. *Band Theory and Electronic Properties of Solids*, volume 2. Oxford University Press, 2001.